J. Fluid Mech. (1985), *vol.* 152, *pp.* 217–233
Printed in Great Britain

Contaminant dispersion as viewed from a fixed position

By RONALD SMITH

Department of Applied Mathematics and Theoretical Physics, University of Cambridge, Silver Street, Cambridge CB3 9EW

(Received 17 February 1984 and in revised form 3 October 1984)

A Hermite series expansion is used to describe the time evolution of the contaminant concentration at a fixed location in a flow. Exact expressions are derived for the dosage, centroid and temporal variance. A two-mode approximation is proposed which gives accurate results at moderate to large distances downstream of the discharge.

1. Introduction

By tradition, and for analytic tractability, theoretical studies of contaminant dispersion generally concern the spatial distribution of concentration. For similarly compelling reasons, such as limitations upon the available number of measuring stations, experimental studies usually lead to data for the temporal distribution of concentration. Therefore approximations, of a variety of levels of sophistication (Chatwin 1971), have had to be made when comparing (spatial) analytical predictions with (temporal) experimental results.

An important theoretical development was made by Tsai & Holley (1978) when they showed that it was possible to calculate numerically the temporal moments of the concentration at a fixed location. Chatwin (1980) demonstrated how such information of the first few moments can be used to construct accurate Hermite series approximations to the temporal distribution.

The starting point for the present paper is a modification of the method of Tsai & Holley (1978) so that direct predictions are made for the temporal contaminant distribution in the manner advocated by Chatwin (1980). Then, rather than obtaining numerical solutions, exact expressions are derived for the dosage, centroid and temporal variance. Alas, these expressions are no less complicated than the corresponding spatial results (Aris 1956; Chatwin 1970; Smith 1982*a*). Guided by the form of the exact solutions, a simple yet accurate approximation is proposed.

2. Hermite series representation

Shear dispersion, as contrasted to the direct effects of longitudinal diffusion, is of importance only in high Peclet number (laminar or turbulent) flows. Thus, following the practice established by G. I. Taylor (1953), we shall neglect the effect of longitudinal diffusion. We shall also make the simplifying assumption that the flow is longitudinally uniform (independent of x). Hence, the advection-diffusion equation for the contaminant concentration $c(x, y, z, t)$ takes the form

$$\partial_t c + u\,\partial_x c = \nabla\cdot(\boldsymbol{\kappa}\cdot\nabla c), \tag{2.1a}$$

with $$\boldsymbol{n}\cdot\boldsymbol{\kappa}\cdot\boldsymbol{\nabla}c = 0 \quad \text{on } \partial A, \tag{2.1b}$$

and $$uc = q(y,z)\,\delta(t) \quad \text{at } x = 0. \tag{2.1c}$$

Here $u(y,z)$ is the longitudinal velocity, $\boldsymbol{\kappa}(y,z)$ the transverse diffusivity tensor, $\boldsymbol{\nabla}$ the transverse gradient operator $(0, \partial_y, \partial_z)$, ∂A the impermeable boundary, $\boldsymbol{n}$ the outward normal, and $q(y,z)$ the discharge profile.

Guided by the work of Chatwin (1970, 1980) and of Smith (1982*a*), we represent $c(x,y,z,t)$ by a temporal Hermite series expansion:

$$c = \frac{1}{(2\pi)^{\frac{1}{2}}\sigma}\exp(-\tfrac{1}{2}\xi^2)\left\{a^{(0)} + \sum_{m=3}^{\infty}\frac{a^{(m)}}{\sigma^m}\,\mathrm{He}_m(\xi)\right\}, \tag{2.2a}$$

with $$\xi = \{t-T\}/\sigma. \tag{2.2b}$$

Here $T(x,y,z)$ is the temporal centroid, and $\sigma^2(x,y,z)$ the temporal variance of the contaminant cloud, as observed at the location (x,y,z). The Hermite polynomials He_m are defined recursively:

$$\mathrm{He}_0 = 1, \quad \mathrm{He}_1 = \xi, \quad \mathrm{He}_{m+2} = \xi\,\mathrm{He}_{m+1} - (m+1)\,\mathrm{He}_m \quad \text{for } m \geqslant 0. \tag{2.3}$$

The rate of convergence of (2.2*a*) depends upon how close to Gaussian is the temporal concentration distribution at a fixed position (x,y,z). The work of Chatwin (1970, 1980) suggests that this becomes better as x increases. Thus the present work can be regarded as being most pertinent at moderate or large distances downstream of a discharge.

In effect the representation (2.2*a*) factors out the t-dependence. The functions $a^{(0)}$, T, σ^2, ... are functions of position (x,y,z). The equations that they satisfy can be derived by our taking the He_m component of the advection-diffusion equation (2.1*a*):

$$\begin{aligned} &u\,\partial_x a^{(m)} - \boldsymbol{\nabla}\cdot(\boldsymbol{\kappa}\cdot\boldsymbol{\nabla}a^{(m)}) \\ &\quad = a^{(m-1)} - a^{(m-1)}u\,\partial_x T + \boldsymbol{\kappa}:\boldsymbol{\nabla}T\,\boldsymbol{\nabla}a^{(m-1)} + \boldsymbol{\nabla}\cdot(\boldsymbol{\kappa}\cdot a^{(m-1)}\,\boldsymbol{\nabla}T) \\ &\qquad + \tfrac{1}{2}\{\boldsymbol{\kappa}:\boldsymbol{\nabla}\sigma^2\,\boldsymbol{\nabla}a^{(m-2)} + \boldsymbol{\nabla}\cdot(\boldsymbol{\kappa}\cdot a^{(m-2)}\,\boldsymbol{\nabla}\sigma^2) - a^{(m-2)}u\,\partial_x\sigma^2 + 2a^{(m-2)}\boldsymbol{\kappa}:(\boldsymbol{\nabla}T)^2\} \\ &\qquad + a^{(m-3)}\boldsymbol{\kappa}:\boldsymbol{\nabla}T\,\boldsymbol{\nabla}\sigma^2 + \tfrac{1}{4}a^{(m-4)}\boldsymbol{\kappa}:(\boldsymbol{\nabla}\sigma^2)^2, \end{aligned} \tag{2.4a}$$

with $$\boldsymbol{n}\cdot\boldsymbol{\kappa}\cdot\boldsymbol{\nabla}a^{(m)} = -a^{(m-1)}\boldsymbol{n}\cdot\boldsymbol{\kappa}\cdot\boldsymbol{\nabla}T - \tfrac{1}{2}a^{(m-2)}\boldsymbol{n}\cdot\boldsymbol{\kappa}\cdot\boldsymbol{\nabla}\sigma^2 \quad \text{on } \partial A, \tag{2.4b}$$

and $$a^{(0)} = q/u, \quad 0 = T = \sigma^2 = a^{(3)} = \ldots \quad \text{at } x = 0. \tag{2.4c}$$

3. Advection-diffusion eigenmodes

For $m = 0$ the equations (2.4*a–c*) take the form

$$u\,\partial_x a^{(0)} - \boldsymbol{\nabla}\cdot(\boldsymbol{\kappa}\cdot\boldsymbol{\nabla}a^{(0)}) = 0, \tag{3.1a}$$

with $$\boldsymbol{n}\cdot\boldsymbol{\kappa}\cdot\boldsymbol{\nabla}a^{(0)} = 0 \quad \text{on } \partial A, \tag{3.1b}$$

and $$a^{(0)} = q/u \quad \text{at } x = 0. \tag{3.1c}$$

Close to the discharge position we have the Taylor series approximation

$$a^{(0)} = \left(\frac{q}{u}\right) + \frac{x}{u}\,\boldsymbol{\nabla}\cdot\left(\boldsymbol{\kappa}\cdot\boldsymbol{\nabla}\left(\frac{q}{u}\right)\right) + O(x^2). \tag{3.2}$$

To obtain the full solution of equations (3.1*a–c*) we introduce the advection-diffusion eigenmodes $\phi_n(y,z)$:

$$\nabla\cdot(\kappa\cdot\nabla\phi_n)+\mu_n u\phi_n = 0, \tag{3.3a}$$

with

$$n\cdot\kappa\cdot\nabla\phi_n = 0 \quad \text{on } \partial A. \tag{3.3b}$$

and

$$\overline{u\phi_n^2} = \bar{u},\ \overline{u\phi_m\phi_n} = 0 \quad \text{for } m \neq n, \tag{3.3c,d}$$

(Tsai & Holley, 1978; Smith 1982*b*), where the over-bars denote the cross-sectional average values. The normalization (3.3*c*) ensures that the lowest mode is

$$\phi_0 = 1 \quad \text{with } \mu_0 = 0. \tag{3.4}$$

In terms of the eigenmodes the starting value can be represented

$$q(y,z) = \frac{u(y,z)}{\bar{u}}\left[\bar{q}+\sum_{n=1}^{\infty}\overline{q\phi_n}\,\phi_n(y,z)\right] \tag{3.5}$$

(e.g. multiply both sides by ϕ_m and integrate, making use of the identities (3.3*c,d*)). This leads to the solution

$$a^{(0)} = \left[\bar{q}+\sum_{n=1}^{\infty}\overline{q\phi_n}\exp(-\mu_n x)\,\phi_n(y,z)\right]\Big/\bar{u} \tag{3.6}$$

(Tsai & Holley 1978, equation 14). Thus the zero temporal moment becomes uniform across the flow on a length scale of order $1/\mu_1$ downstream of the discharge. (For non-conserved contaminants the lowest mode ϕ_0 is not uniform, and the asymptote is to the modal shape ϕ_0). If the discharge has the same shape as the velocity profile (i.e. $\overline{q\phi_n} \propto \overline{u\phi_0\phi_n} = 0$) then for conserved contaminants $a^{(0)}$ is uniform for all x.

In view of the result

$$a^{(0)}(x,y,z) = \int_{-\infty}^{\infty} c(x,y,z,t)\,\mathrm{d}t, \tag{3.7}$$

we can interpret $a^{(0)}$ as being the total dosage at the location (x,y,z). The work of Smith (1982*b*) can be interpreted as concerning the dosage experienced at the shoreline of a shallow river. The optimal site for a point discharge is at the zero crossing of the first advection-diffusion eigenmode ϕ_1. For this unique discharge site the dosage $a^{(0)}$ at either river bank never exceeds the asymptotic value $\bar{q}/\bar{u}$, i.e. is just as good as the more expensive strategy of matching the discharge to the volume flow rate ($\overline{q\phi_n} = 0$).

4. Temporal centroid

For $m = 1$ the absence of $a^{(1)}$ in the representation (2.2*a*) means that (2.4*a–c*) yield equations for the centroid $T(x,y,z)$:

$$u\,\partial_x(a^{(0)}T)-\nabla\cdot(\kappa\cdot\nabla(a^{(0)}T)) = a^{(0)}, \tag{4.1a}$$

with

$$n\cdot\kappa\cdot\nabla(a^{(0)}T) = 0 \quad \text{on } \partial A, \tag{4.1b}$$

and

$$T = 0 \quad \text{at } x = 0. \tag{4.1c}$$

Close to the discharge we obtain the intuitively obvious result that the time-of-arrival varies inversely as the local flow velocity

$$T = x/u+O(x^2). \tag{4.2}$$

To solve (4.1*a*–c) in terms of the eigenmodes $\phi_n(y,z)$, we note the series representations:

$$1 = \frac{u}{\bar{u}}\left[1 + \sum_{n=1}^{\infty} \overline{\phi_n}\,\phi_n\right], \tag{4.3a}$$

$$\phi_m = \frac{u}{\bar{u}}\left[\overline{\phi_m} + \sum_{n=1}^{\infty} \overline{\phi_m\,\phi_n}\,\phi_n\right]. \tag{4.3b}$$

Thus, we can formally represent the right-hand side term in equation (4.1*a*):

$$a^{(0)} = \frac{u}{\bar{u}^2}\left[\bar{q} + \sum_{m=1}^{\infty} \overline{q\phi_m}\;\overline{\phi_m}\exp(-\mu_m x)\right] + \frac{u}{\bar{u}^2}\sum_{n=1}^{\infty}\phi_n\left[\overline{\phi_n}\,\bar{q} + \sum_{m=1}^{\infty}\overline{q\phi_m}\;\overline{\phi_m\phi_n}\exp(-\mu_m x)\right]. \tag{4.4}$$

Solving equations (4.1*a*–c) for each eigenmode separately we derive the composite solution

$$\begin{aligned}\bar{u}^2 a^{(0)} T = \bar{q}\Bigg[x &+ \sum_{n=1}^{\infty}\phi_n\overline{\phi_n}\frac{(1-\exp(-\mu_n x))}{\mu_n}\Bigg] \\ &+ \sum_{m=1}^{\infty}\overline{q\phi_m}\;\overline{\phi_m}\frac{(1-\exp(-\mu_m x))}{\mu_m} + \sum_{n=1}^{\infty}\phi_n\,\overline{q\phi_n}\;\overline{\phi_n^2}\,x\exp(-\mu_n x) \\ &+ \sum_{n=1}^{\infty}\phi_n\sum_{m\neq n}\overline{q\phi_m}\;\overline{\phi_m\phi_n}\frac{[\exp(-\mu_n x)-\exp(-\mu_m x)]}{\mu_n-\mu_m}.\end{aligned} \tag{4.5}$$

The pointwise convergence of the series (3.5, 4.3*a*, *b*) is not rapid, with the consequence that for small x neither is (3.6, 4.5). As x increases the exponential and $1/\mu_n$ factors greatly accelerate the convergence of the series for $a^{(0)}$ and T.

From this full solution (4.5) we can re-derive the asymptotic results obtained by Smith (1984, §4). First we note that for large x we have

$$T \approx \frac{x}{\bar{u}} + G(y,z) + \frac{\overline{qG}}{\bar{q}}, \tag{4.6a}$$

where

$$G(y,z) = \frac{1}{\bar{u}}\sum_{n=1}^{\infty}\frac{\phi_n(y,z)\,\overline{\phi_n}}{\mu_n}. \tag{4.6b}$$

Thus, the contaminant cloud eventually moves at the bulk velocity $\bar{u}$, with a shift of time $G(y,z)$ between streamlines. There is an additional forwards or backwards time displacement if the discharge or monitoring position is in a part of the flow where $G(y,z)$ is positive or negative respectively. Next, making use of the equations (3.3*a*–c, 4.3*a*) satisfied by the eigenmodes $\phi_n(y,z)$, we can confirm that the summation (4.6*b*) is a solution of the transverse diffusion equation

$$\nabla\cdot(\boldsymbol{\kappa}\cdot\nabla G) = -\left(1-\frac{u}{\bar{u}}\right), \tag{4.7a}$$

with

$$\boldsymbol{n}\cdot\boldsymbol{\kappa}\cdot\nabla G = 0 \quad \text{on } \partial A, \tag{4.7b}$$

and

$$\overline{uG} = 0 \tag{4.7c}$$

(Smith 1984, equations (4.3*a*–c)).

For later use we note the results

$$\bar{G} = \frac{1}{\bar{u}} \sum_{n=1}^{\infty} \frac{\overline{\phi_n^2}}{\mu_n}, \tag{4.8a}$$

$$\overline{uG^2} = \frac{1}{\bar{u}} \sum_{n=1}^{\infty} \frac{\overline{\phi_n^2}}{\mu_n^2}, \tag{4.8b}$$

$$\left(1-\frac{u}{\bar{u}}\right) G - \frac{u}{\bar{u}} \bar{G} = \frac{u}{\bar{u}} \left\{ \sum_{n=1}^{\infty} \phi_n \frac{\overline{\phi_n}}{\mu_n} (\overline{\phi_n}^2 - 1) + \sum_{n=1}^{\infty} \phi_n \sum_{m \neq n} \frac{\overline{\phi_m}}{\mu_m} \overline{\phi_m \phi_n} \right\}. \tag{4.8c}$$

Inevitably, there are many close similarities to the long-established spatial description of contaminant dispersion. For example, Aris (1956, equations 18, 23) gives the spatial counterparts of (3.6, 4.5). The differences arise in the definitions of the respective eigenmodes. At large times there is a shift $g(y,z)$ of the spatial centre-of-gravity between streamlines (Aris 1956, equation 24; Chatwin 1970, equation 1.9). Except for a $1/\bar{u}$ factor and the choice of normalization (4.7*c*), $g(y,z)$ satisfies the same equations as the shift of time $G(y,z)$. As noted by Smith (1984, equation 11.3) the relationship can be written

$$G = \frac{\overline{ug} - \bar{u}g}{\bar{u}^2}, \quad g = \bar{u}(\bar{G} - G). \tag{4.9}$$

5. Variance

For $m = 2$ (2.4*a–c*) can be re-written:

$$u\,\partial_x(a^{(0)}\sigma^2) - \boldsymbol{\nabla}\cdot(\boldsymbol{\kappa}\cdot\boldsymbol{\nabla}(a^{(0)}\sigma^2)) = 2a^{(0)}\boldsymbol{\kappa} : (\boldsymbol{\nabla}T)^2, \tag{5.1a}$$

with
$$\boldsymbol{n}\cdot\boldsymbol{\kappa}\cdot\boldsymbol{\nabla}(a^{(0)}\sigma^2) = 0 \quad \text{on } \partial A, \tag{5.1b}$$

and
$$a^{(0)}\sigma^2 = 0 \quad \text{at } x = 0. \tag{5.1c}$$

Making use of (3.2, 4.2), we infer that σ^2 initially grows as x^3:

$$\sigma^2 = \tfrac{2}{3}x^3\boldsymbol{\kappa} : (\boldsymbol{\nabla}u)^2/u^5 + O(x^4). \tag{5.2}$$

Thus, strong shear or low velocities are associated with comparatively large dilution. Commonly, both these contributory factors are strongest close to boundaries.

The quadratic dependence of $(\boldsymbol{\nabla}T)^2$ upon q makes equation (5.1*a*) awkward to solve directly. To avoid this difficulty we follow Smith (1982*a*) and make the change of dependent variable:

$$a^{(0)}\sigma^2 = V - a^{(0)}\left(T - \frac{x}{\bar{u}}\right)^2. \tag{5.3}$$

The equation for V is

$$u\,\partial_x V - \boldsymbol{\nabla}\cdot(\boldsymbol{\kappa}\cdot\boldsymbol{\nabla}V) = 2\left(1-\frac{u}{\bar{u}}\right)\left(a^{(0)}T - \frac{a^{(0)}x}{\bar{u}}\right), \tag{5.4a}$$

with
$$\boldsymbol{n}\cdot\boldsymbol{\kappa}\cdot\boldsymbol{\nabla}V = 0 \quad \text{on } \partial A, \tag{5.4b}$$

and
$$V = 0 \quad \text{at } x = 0. \tag{5.4c}$$

If we represent the second moment $V(x,y,z)$ by an eigen-function expansion

$$V = V_0(x) + \sum_{n=1}^{\infty} V_n(x)\,\phi_n(y,z), \tag{5.5}$$

then we can replace equations (5.4*a–c*) by the sequence of first-order ordinary differential equations

$$\frac{\mathrm{d}V_0}{\mathrm{d}x} = 2\frac{\bar{q}}{\bar{u}^3}\sum_{n=1}^{\infty}\overline{\phi_n}^2(1-\exp(-\mu_n x)) + \frac{2}{\bar{u}^3}\sum_{n=1}^{\infty}\overline{q\phi_n}\,\overline{\phi_n}\,(\overline{\phi_n}^2-1)\,x\exp(-\mu_n x) + \frac{2}{\bar{u}^3}\sum_{n=1}^{\infty}\sum_{m\neq n}\overline{q\phi_m}\,\overline{\phi_n}\,\overline{\phi_n\phi_m}\,\frac{[\exp(-\mu_n x)-\exp(-\mu_m x)]}{\mu_m-\mu_n}, \tag{5.6a}$$

$$\frac{\mathrm{d}V_n}{\mathrm{d}x}+\mu_n V_n = 2\frac{\bar{q}}{\bar{u}^3}\left\{(\overline{\phi_n^2}-1)\,\overline{\phi_n}\,\frac{(1-\exp(-\mu_n x))}{\mu_n}+\sum_{m\neq n}\overline{\phi_m}\,\overline{\phi_m\phi_n}\,\frac{(1-\exp(-\mu_m x))}{\mu_m}\right\} + 2\frac{\overline{\phi_n}}{\bar{u}^3}\sum_{m=1}^{\infty}\overline{q\phi_m}\,\overline{\phi_m}\,\frac{(1-\exp(-\mu_m x))}{\mu_m}+2\frac{\overline{q\phi_n}}{\bar{u}^3}(\overline{\phi_n^2}-1)\,x\exp(-\mu_n x) + \frac{2}{\bar{u}^3}\sum_{m\neq n}\overline{q\phi_m}\,\overline{\phi_m\phi_n}\,(\overline{\phi_m^2}-1)\,x\exp(-\mu_m x) + \frac{2}{\bar{u}^3}(\overline{\phi_n^2}-1)\sum_{m\neq n}\overline{q\phi_m}\,\overline{\phi_m\phi_n}\,\frac{[\exp(-\mu_n x)-\exp(-\mu_m x)]}{\mu_m-\mu_n} + \frac{2}{\bar{u}^3}\overline{q\phi_n}\sum_{m\neq n}\overline{\phi_m\phi_n}^2\,\frac{[\exp(-\mu_n x)-\exp(-\mu_m x)]}{\mu_m-\mu_n} + \frac{2}{\bar{u}^3}\sum_{m\neq n}\sum_{\substack{p\neq m\\ p\neq n}}\overline{\phi_m\phi_n}\,\overline{\phi_p\phi_m}\,\overline{q\phi_p}\,\frac{[\exp(-\mu_m x)-\exp(-\mu_p x)]}{\mu_p-\mu_m}. \tag{5.6b}$$

The solutions for the modal weight factors are

$$V_0 = 2\frac{\bar{q}}{\bar{u}^3}\left\{x\sum_{n=1}^{\infty}\frac{\overline{\phi_n}^2}{\mu_n}-\sum_{n=1}^{\infty}\overline{\phi_n}^2\,\frac{(1-\exp(-\mu_n x))}{\mu_n^2}\right\} + \frac{2}{\bar{u}^3}\sum_{n=1}^{\infty}\overline{q\phi_n}\,\overline{\phi_n}\,\frac{(\overline{\phi_n^2}-1)}{\mu_n^2}\,[1-(\mu_n x+1)\exp(-\mu_n x)] + \frac{2}{\bar{u}^3}\sum_{n=1}^{\infty}\sum_{m\neq n}\overline{q\phi_m}\,\overline{\phi_n}\,\frac{\overline{\phi_m\phi_n}}{\mu_m\mu_n}\left[1-\frac{\mu_m\exp(-\mu_n x)-\mu_n\exp(-\mu_m x)}{\mu_m-\mu_n}\right], \tag{5.7a}$$

$$V_n = 2\frac{\bar{q}}{\bar{u}^3}\left\{\frac{(\overline{\phi_n^2}-1)\,\overline{\phi_n}}{\mu_n^2}\,[1-(\mu_n x+1)\exp(-\mu_n x)] + \sum_{m\neq n}\frac{\overline{\phi_m\phi_n}\,\overline{\phi_m}}{\mu_m\mu_n}\left[1-\frac{\mu_m\exp(-\mu_n x)-\mu_n\exp(-\mu_m x)}{\mu_m-\mu_n}\right]\right\} + \frac{\overline{q\phi_n}}{\bar{u}^3}(\overline{\phi_n^2}-1)^2x^2\exp(-\mu_n x)+2\frac{\overline{q\phi_n}\,\overline{\phi_n}^2}{\bar{u}^3\mu_n^2}\,[1-(\mu_n x+1)\exp(-\mu_n x)] + 2\frac{\overline{\phi_n}}{\bar{u}^3}\sum_{m\neq n}\frac{\overline{q\phi_m}\,\overline{\phi_m}}{\mu_m\mu_n}\left[1-\frac{\mu_m\exp(-\mu_n x)-\mu_n\exp(-\mu_m x)}{\mu_m-\mu_n}\right] - \frac{2}{\bar{u}^3}\sum_{m\neq n}\overline{q\phi_m}\,\frac{\overline{\phi_m\phi_n}(\overline{\phi_m^2}-1)}{\mu_m-\mu_n}\left[x\exp(-\mu_m x)-\frac{\exp(-\mu_n x)-\exp(-\mu_m x)}{\mu_m-\mu_n}\right]$$

$$+2\frac{(\overline{\phi_n^2}-1)}{\bar{u}^3}\sum_{m\neq n}\frac{\overline{q\phi_m}\,\overline{\phi_m\phi_n}}{\mu_m-\mu_n}\left[x\exp(-\mu_n x)-\frac{\exp(-\mu_n x)-\exp(-\mu_m x)}{\mu_m-\mu_n}\right]$$

$$+2\frac{\overline{q\phi_n}}{\bar{u}^3}\sum_{m\neq n}\frac{\overline{\phi_m\phi_n}^2}{\mu_m-\mu_n}\left[x\exp(-\mu_n x)-\frac{\exp(-\mu_n x)-\exp(-\mu_m x)}{\mu_m-\mu_n}\right]$$

$$+\frac{2}{\bar{u}^3}\sum_{m\neq n}\sum_{\substack{p\neq m\\ p\neq n}}\frac{\overline{\phi_m\phi_n}\,\overline{\phi_p\phi_m}\,\overline{q\phi_p}}{\mu_p-\mu_m}\left\{\frac{\exp(-\mu_n x)-\exp(-\mu_m x)}{\mu_m-\mu_n}\right.$$

$$\left.-\frac{\exp(-\mu_n x)-\exp(-\mu_p x)}{\mu_p-\mu_n}\right\}. \qquad (5.7b)$$

We observe that for small x the coefficients V_0, V_n grow as x^2, as contrasted to the slower x^3 growth of σ^2 (although in this limit the convergence of the series is exceedingly slow).

Again, we can use this full solution (5.5; 5.7*a*, *b*) to re-derive the asymptotic results obtained by Smith (1984, §§§5–7). For the ϕ_0 weight factor we have (see 4.8*a*, *b*):

$$V_0 \sim \frac{2\bar{q}}{\bar{u}^2}\{x\bar{G}-\overline{uG^2}\}+\frac{2}{\bar{u}}\overline{qG^{(2)}}, \qquad (5.8a)$$

where

$$\bar{u}^2G^{(2)}(y,z)=\sum_{n=1}^{\infty}(\overline{\phi_n^2}-1)\frac{\overline{\phi_n}}{\mu_n^2}\phi_n(y,z)+\sum_{n=1}^{\infty}\frac{\phi_n(y,z)}{\mu_n}\sum_{m\neq n}\frac{\overline{\phi_m}}{\mu_m}\overline{\phi_m\phi_n}. \qquad (5.8b)$$

The $1/\mu_n\mu_m$ factors make the convergence extremely rapid. From (4.8*c*) we can confirm that, in agreement with (6.7*a*–*c*) of Smith (1984), the auxiliary function $G^{(2)}$ satisfies the transverse diffusion equation

$$\nabla\cdot(\boldsymbol{\kappa}\cdot\nabla G^{(2)})=\frac{u}{\bar{u}}\bar{G}-\left(1-\frac{u}{\bar{u}}\right)G, \qquad (5.9a)$$

with

$$\boldsymbol{n}\cdot\boldsymbol{\kappa}\cdot\nabla G^{(2)}=0 \quad \text{on } \partial A, \qquad (5.9b)$$

and

$$\overline{uG^{(2)}}=0. \qquad (5.9c)$$

Conveniently, the asymptotic form of the series for the higher coefficients involves the same auxiliary function $G^{(2)}$:

$$\sum_{n=1}^{\infty}V_n(x)\phi_n(y,z)\sim 2\frac{\bar{q}}{\bar{u}}G^{(2)}(y,z)+\frac{2}{\bar{u}}\overline{qG}\,G(y,z) \qquad (5.10)$$

(Smith 1984, equation 7.2). We note that from (4.7, 5.9) it can be shown that

$$\bar{u}\overline{G^{(2)}}=\overline{(\bar{u}-u)G^2}, \qquad (5.11a)$$

$$\overline{(\bar{u}-u)GG^{(2)}}=\overline{\kappa(\nabla G^{(2)})^2}. \qquad (5.11b)$$

For the temporal variance σ^2 the resulting asymptotic expression is

$$\sigma^2\sim\frac{2x\bar{G}}{\bar{u}}-\frac{2\overline{uG^2}}{\bar{u}}+2\left(\frac{\overline{qG^{(2)}}}{\bar{q}}\right)-\left(\frac{\overline{qG}}{\bar{q}}\right)^2+2G^{(2)}(y,z)-G(y,z)^2 \qquad (5.12)$$

(Smith 1984, equation 7.4). The linear growth rate with distance is related to the shear-dispersion coefficient (Smith 1984, equation 5.4):

$$\frac{\partial \sigma^2}{\partial x} \sim \frac{2}{\bar{u}^3} D(\infty) \quad \text{where } D(\infty) = \bar{u}^2 \bar{G}. \tag{5.13}$$

This is, of course, equivalent to the spatial result derived first by G. I. Taylor (1953)

$$D(\infty) = \overline{ug}. \tag{5.14}$$

6. Two-mode approximation

The exact solutions for the centroid and for the variance are formidably complicated. Indeed, Tsai & Holley (1978) advocate the use of numerical rather than analytical solutions for the temporal moments. Of course, for small and for large distances downstream of the discharge we have the respective asymptotic formulae (4.2, 5.2) and (4.6, 5.11). However, there is a need for some simple approximations applicable to intermediate distances.

One limiting case in which the exact solutions are themselves simple is when there is only a small number of modes $\phi_1(y,z), \ldots, \phi_N(y,z)$ e.g. for a flow with 2 or 3 well-mixed cells the modes describe the approach to uniformity of concentration imbalances between the cells (Thacker 1976). In particular, if we are to reproduce the large x asymptotes (4.6a, 5.8a, 5.10) then we need a minimum of two ortho-normal modes:

$$\bar{u}G(y,z) = \frac{\phi_1(y,z)}{\mu_1}\overline{\phi_1} + \frac{\phi_2(y,z)}{\mu_2}\overline{\phi_2}, \tag{6.1a}$$

$$\bar{u}^2 G^{(2)}(y,z) = \frac{\phi_1(y,z)}{\mu_1}\overline{(\bar{u}-u)G\phi_1} + \frac{\phi_2(y,z)}{\mu_2}\overline{(\bar{u}-u)G\phi_2} \tag{6.1b}$$

(c.f. the definitions (4.6b, 5.8b) of $G, G^{(2)}$). In effect we are seeking to replace the actual source and velocity profiles $q(y,z)$ and $u(y,z)$ by analytically convenient forms which involve two optimally chosen non-uniform modes.

It follows from equations (6.1 a, b) that ϕ_1, ϕ_2 can be expressed as linear combinations of $G, G^{(2)}$. For algebraic convenience we write these combinations:

$$\phi_j = \frac{\alpha_j[(\bar{u}-u)G\overline{G^{(2)}}\bar{u}\overline{G} - \bar{u}\overline{G^{(2)}}\bar{u}\overline{G^{(2)}}]}{[(\bar{u}-u)G\overline{G^{(2)}}\bar{u}\overline{G} - (\bar{u}\overline{G^{(2)}})^2]} + \frac{\beta_j[\overline{G}\bar{u}\overline{G^{(2)}} - \bar{u}\overline{G^{(2)}}\overline{G}]}{[(\bar{u}-u)G\overline{G^{(2)}}\bar{u}\overline{G} - (\bar{u}\overline{G^{(2)}})^2]} \quad j = 1,2, \tag{6.2}$$

where the coefficients α_1, α_2, β_1, β_2 remain to be determined. Substituting back into equations (6.1 a, b) and extracting the coefficients of G, $\bar{u}G^{(2)}$ we find that

$$\frac{\alpha_1^2}{\mu_1} + \frac{\alpha_2^2}{\mu_2} = \bar{u}\overline{G}, \quad \frac{\alpha_1\beta_1}{\mu_1} + \frac{\alpha_2\beta_2}{\mu_2} = \bar{u}^2\overline{G^{(2)}}, \quad \frac{\beta_1^2}{\mu_1} + \frac{\beta_2^2}{\mu_2} = \bar{u}^2\overline{(\bar{u}-u)GG^{(2)}}. \tag{6.3a,b,c}$$

Also, from the expressions

$$\bar{u}G = \frac{\alpha_1\phi_1}{\mu_1} + \frac{\alpha_2\phi_2}{\mu_2}, \quad \bar{u}^2 G^{(2)} = \frac{\beta_1\phi_1}{\mu_1} + \frac{\beta_2\phi_2}{\mu_2}, \tag{6.4a,b}$$

we can use the ortho-normality (3.3c, d) to infer the further three relationships

$$\frac{\alpha_1^2}{\mu_1^2} + \frac{\alpha_2^2}{\mu_2^2} = \overline{\bar{u}uG^2}, \quad \frac{\alpha_1\beta_1}{\mu_1^2} + \frac{\alpha_2\beta_2}{\mu_2^2} = \overline{\bar{u}^2 uGG^{(2)}}, \quad \frac{\beta_1^2}{\mu_1^2} + \frac{\beta_2^2}{\mu_2^2} = \overline{\bar{u}^3 uG^{(2)2}}. \tag{6.5a,b,c}$$

Solving for α_j^2, $\alpha_j\beta_j$, β_j^2 we find that

$$\alpha_1^2 = \frac{\bar{u}\mu_1^2}{\mu_2-\mu_1}[\mu_2\,\overline{uG^2}-\bar{G}], \quad \alpha_2^2 = \frac{\bar{u}\mu_2^2}{\mu_2-\mu_1}[\bar{G}-\mu_1\,\overline{uG^2}], \tag{6.6a,b}$$

$$\alpha_1\beta_1 = \frac{\bar{u}\mu_1^2}{\mu_2-\mu_1}[\mu_2\,\overline{uuGG^{(2)}}-\overline{uG^{(2)}}], \quad \alpha_2\beta_2 = \frac{\bar{u}\mu_2^2}{\mu_2-\mu_1}[\overline{uG^{(2)}}-\mu_1\,\overline{uuGG^{(2)}}], \tag{6.6c,d}$$

$$\beta_1^2 = \frac{\bar{u}\mu_1^2}{\mu_2-\mu_1}[\mu_2\,\overline{u^2uG^{(2)2}}-\overline{u(\bar{u}-u)\,GG^{(2)}}], \tag{6.6e}$$

$$\beta_2^2 = \frac{\bar{u}\mu_2^2}{\mu_2-\mu_1}[\overline{u(\bar{u}-u)\,GG^{(2)}}-\mu_1\,\overline{u^2uG^{(2)2}}]. \tag{6.6f}$$

The consistency condition $\alpha_j^2\beta_j^2 = (\alpha_j\beta_j)^2$ yields a quadratic equation for the decay exponents μ_1, μ_2:

$$\begin{aligned}\mu^2[&\overline{uG^2}\,\bar{u}^2\overline{uG^{(2)2}}-\bar{u}^2(\overline{uGG^{(2)}})^2]\\ &-\mu[\bar{G}\bar{u}^2\overline{uG^{(2)2}}+\overline{u(\bar{u}-u)\,GG^{(2)}}\;\overline{uG^2}-2\bar{u}^2\overline{G^{(2)}}\;\overline{uGG^{(2)}}]\\ &+[\bar{G}\bar{u}\overline{(\bar{u}-u)\,GG^{(2)}}-\bar{u}^2(\overline{G^{(2)}})^2]=0.\end{aligned} \tag{6.7}$$

Thus, to apply the two-mode approximation first we must solve equations (4.7, 5.9) for the two auxiliary functions $G(y,z)$ and $G^{(2)}(y,z)$. Next, we need to evaluate the seven integrals

$$\bar{G},\ \overline{uG^2},\ \overline{G^{(2)}},\ \overline{uGG^{(2)}},\ \overline{(\bar{u}-u)\,GG^{(2)}},\ \overline{uG^{(2)2}},\ \overline{G^{(2)2}}. \tag{6.8}$$

Then we solve the quadratic equation (6.7) to obtain the spatial decay rates μ_1, μ_2. The values of the coefficients α_1, β_1, α_2, β_2 follow from (6.6*a–f*), and the modal shapes $\phi_1(y,z)$, $\phi_2(y,z)$ from (6.2). A test of the approximations is given in §8 below.

7. A shallow triangular channel

The timescale for vertical mixing in a flow of depth h and of vertical diffusivity κ_{33} is of order h^2/κ_{33}. Similarly, in a flow of width B the timescale for transverse mixing is of order B^2/κ_{22} where $\kappa_{22} \sim 2\kappa_{33}$ (Fischer 1973, figures 2, 3). Thus, in a shallow channel with $h \ll B$ the vertical and transverse mixing stages can be regarded as being quite distinct. In particular, on the longer transverse mixing scale the contaminant concentration can be taken to be independent of the vertical coordinate z.

Mathematically, this simplifying assumption permits us to integrate-out the z-structure. For example, the eigenmode equations (3.3*a–d*) now become:

$$\frac{\mathrm{d}}{\mathrm{d}y}\left(h\,\|\,\kappa_{22}\,\|\,\frac{\mathrm{d}\phi_n}{\mathrm{d}y}\right)+\mu_n\,h\,\|\,u\,\|\,\phi_n = 0, \tag{7.1a}$$

with

$$h\,\|\,\kappa_{22}\,\|\,\frac{\mathrm{d}\phi_n}{\mathrm{d}y} = 0 \quad \text{on } y = y_{\mathrm{R}}, y_{\mathrm{L}}, \tag{7.1b}$$

and

$$\int_{y_{\mathrm{R}}}^{y_{\mathrm{L}}} h\,\|\,u\,\|\,\phi_n^2\,\mathrm{d}y = \bar{u}\int_{y_{\mathrm{R}}}^{y_{\mathrm{L}}} h\,\mathrm{d}y, \tag{7.1c}$$

$$\int_{y_{\mathrm{R}}}^{y_{\mathrm{L}}} h\,\|\,u\,\|\,\phi_n\,\phi_m\,\mathrm{d}y = 0 \quad \text{for } m \neq n, \tag{7.1d}$$

where $\|\,\kappa_{22}\,\|$ is the vertically-averaged transverse diffusivity and $\|\,u\,\|$ is the vertically-averaged longitudinal velocity.

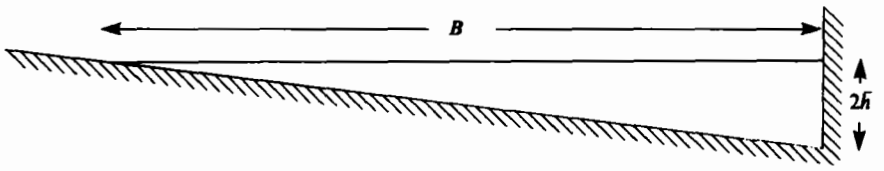

FIGURE 1. Definition sketch of the triangular depth profile.

If the local friction velocity u_* is proportional to the local flow velocity $\| u \|$, then Smith (1984, appendix B) has shown that the velocity and diffusivity distributions can be modelled:

$$\| u \| = \bar{u}h^{\frac{1}{2}}\bar{h}/\overline{h^{\frac{3}{2}}} \quad \| \kappa_{22} \| = \alpha \bar{u}_* \bar{h}h^{\frac{3}{2}}/\overline{h^{\frac{3}{2}}}. \tag{7.2a,b}$$

The empirical constant α has the value 0.15 in straight channel conditions (Fischer 1973). For curving channels the secondary circulation augments transverse mixing and the numerical coefficient can be as large as 0.8. We note that Yotsukura & Sayre (1976) favour a model in which $\| u \|$ varies as $h^{\frac{1}{2}}$, and in the absence of sufficient field data they take $\| \kappa_{22} \|$ to be uniform.

For a triangular channel (see figure 1)

$$h = 2\bar{h}(y/B) \quad (0 < y < B) \tag{7.3}$$

the eigenfunctions are

$$\phi_n = \gamma_n \left\{ \frac{\cos(a_n(y/B)^{\frac{1}{2}})}{(y/B)} - \frac{\sin(a_n(y/B)^{\frac{1}{2}})}{a_n(y/B)^{\frac{1}{2}}} \right\}, \tag{7.4a}$$

with

$$\gamma_n^{-2} = \frac{5}{2}\left\{ 1 + \frac{\cos a_n \sin a_n}{a_n} - \frac{2\sin^2 a_n}{a_n^2} \right\}, \tag{7.4b}$$

$$\mu_n = \tfrac{1}{2}a_n^2(t_c/\bar{u}), \tag{7.4c}$$

and

$$\tan a_n = -3a_n/(a_n^2 - 3), \tag{7.4d}$$

where

$$t_c = B^2/\alpha\bar{h}\bar{u}_* \tag{7.4e}$$

is a characteristic transverse mixing time (Fischer 1973). The first few roots for a_n are

$$a_1 = 5.763, \quad a_2 = 9.095, \quad a_n \sim (n+1)\pi - 3/(n+1)\pi. \tag{7.5}$$

Remembering to include the h weighting factor in the cross-sectional averages, we find that

$$\overline{\phi_n} = 4\gamma_n \left\{ \frac{\sin a_n}{a_n} - \frac{2(1-\cos a_n)}{a_n^2} \right\}, \tag{7.6a}$$

$$\overline{\phi_m \phi_n} = \frac{\gamma_m \gamma_n}{a_m a_n} \{ 2a_m \cos a_m \sin a_n + 2a_n \sin a_m \cos a_n - 2a_m a_n$$
$$- 2\sin a_m \sin a_n + (a_m^2 + a_n^2)[\mathrm{Cin}(a_m + a_n) - \mathrm{Cin}(|a_m - a_n|)] \} \tag{7.6b}$$

where

$$\mathrm{Cin}(a) = \int_0^a \frac{1-\cos\theta}{\theta}\, \mathrm{d}\theta. \tag{7.6c}$$

It now remains for us to evaluate the expressions (3.6, 4.5, 5.7) for the dosage, centroid and variance.

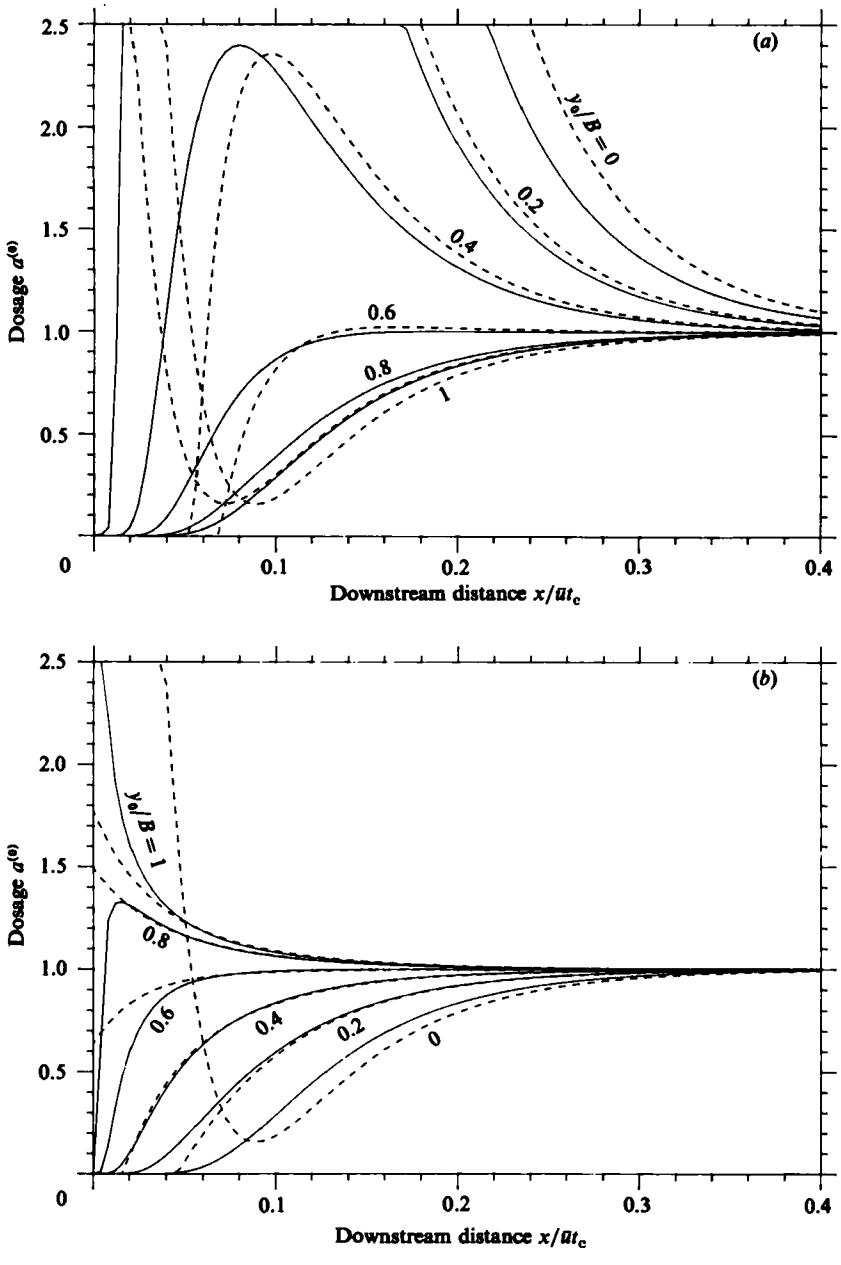

FIGURE 2*a*, *b*. Exact (——) and approximate (----) dosage as functions of downstream position at (*a*) the shallow bank, (*b*) the deep-water bank, for point discharges at various cross-stream locations y_0. t_c is a characteristic transverse mixing time defined in equation (7.4e).

Figure 2(*a*) shows the dosage experienced at the shallow bank $y = 0$ for point discharges of unit vertically integrated strength

$$hq = \delta(y - y_0), \tag{7.7}$$

at a number of cross-stream positions y_0. Figure 2(*b*) gives the corresponding dosages experienced at the deep-water bank $y = B$. We observe that for discharges close to

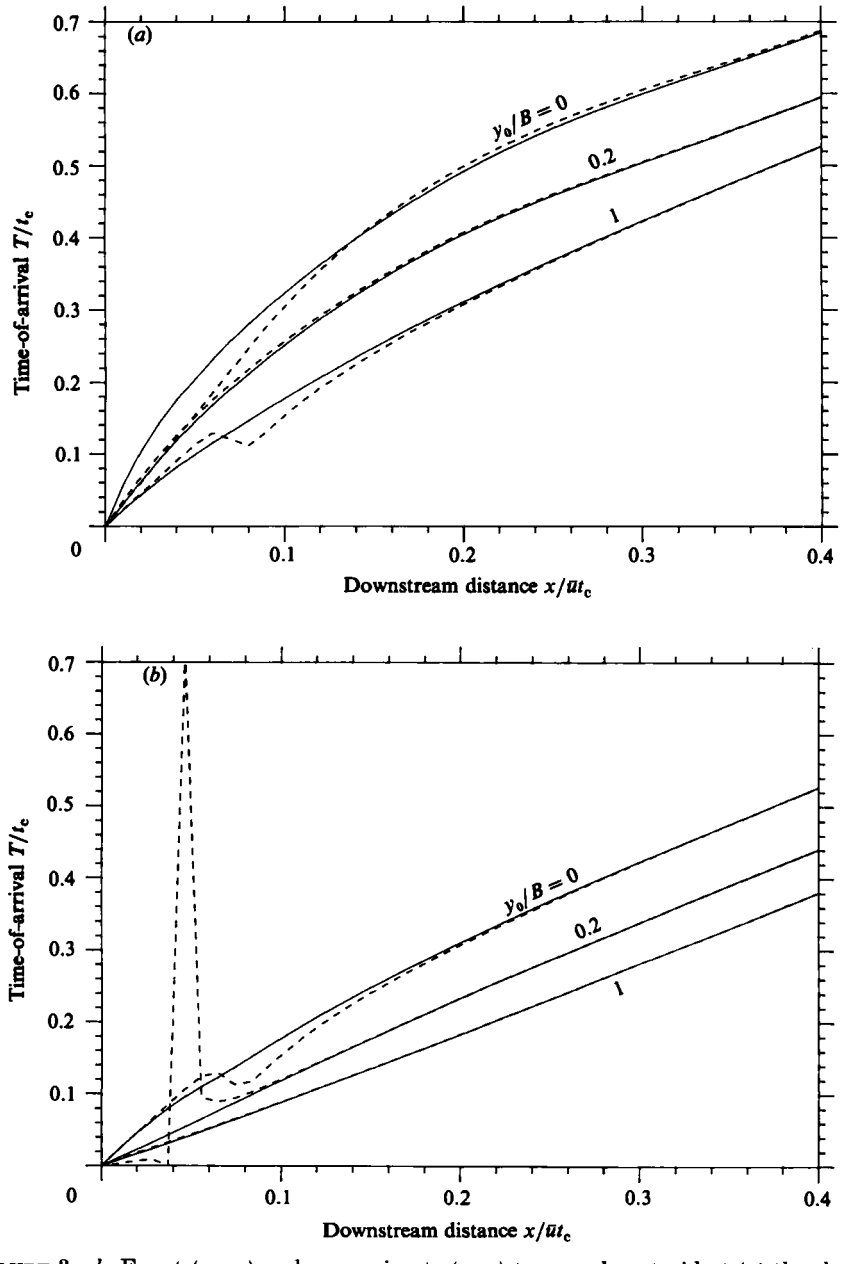

FIGURE 3*a*, *b*. Exact (——) and approximate (----) temporal centroid at (*a*) the shallow bank, (*b*) the deep-water bank.

one of the banks the dosage at the nearby bank increases rapidly downstream and then decreases to the common asymptotic value. Similar features are apparent in figure 3 of Tsai & Holley (1978). The discharge position $y_0/B = 0.6$ is exceptional in so far as at both banks the dosage monotonically increases towards the asymptotic value. This is very close to the optimal discharge site in the sense discussed by Smith (1982*b*).

Figures 3(*a* and *b*) give the results for the temporal centroid T. In accord with

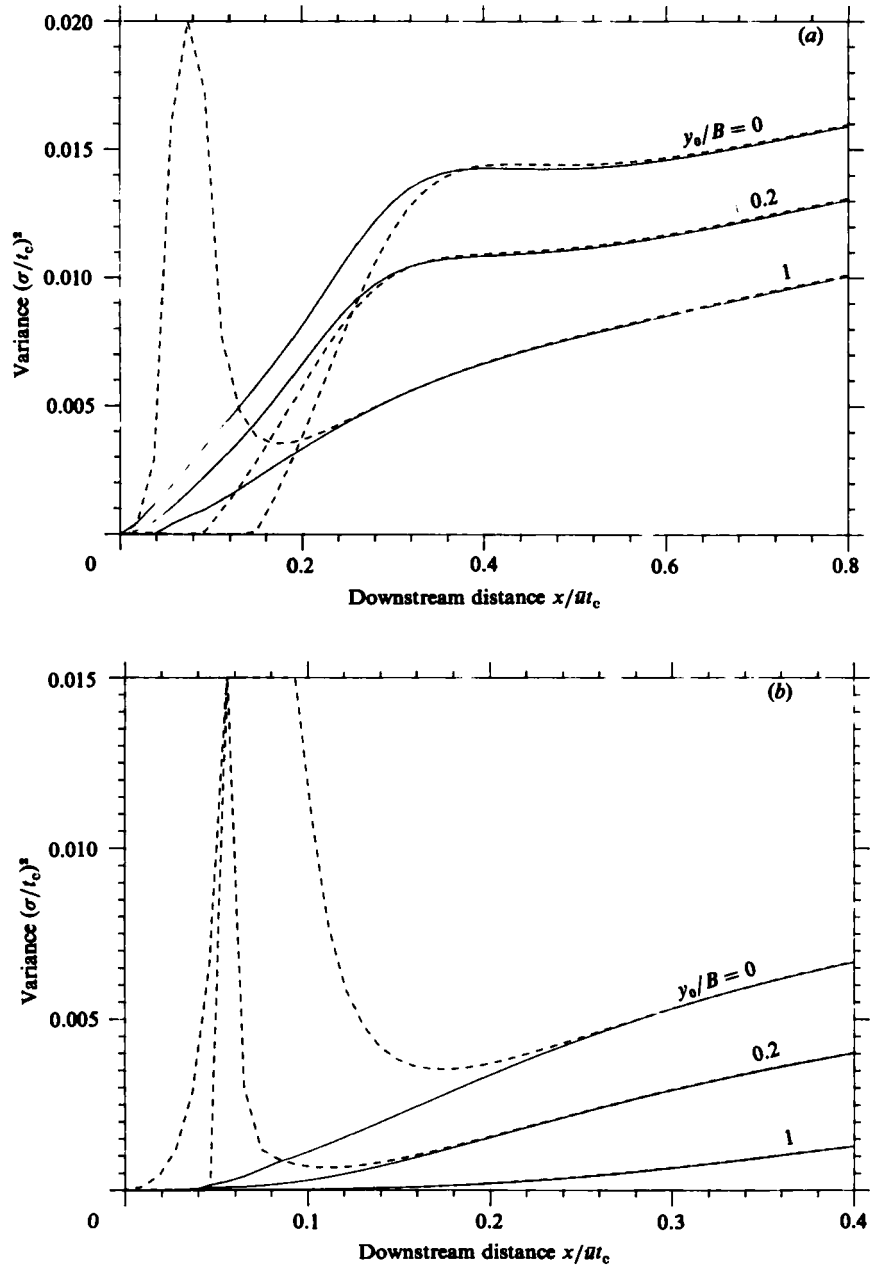

FIGURE 4*a*, *b*. Exact (——) and approximate (----) temporal variance at (*a*) the shallow bank, (*b*) the deep-water bank.

physical intuition, there is a later arrival if either the observations or the discharge are made in a slow-moving part of the flow. A more subtle feature is that the slope can exhibit slight non-monotonicity (e.g. the $y_0/B = 0, 0.2$ curves in figure 3*a*). When the source and observation position are both in the slower-moving water, the effective velocity for the contaminant is initially low. However, at moderate distances downstream the material can have diffused out into the faster-moving part of the

flow, travelled along relatively quickly, and then diffused back to the bank. It is this speeding-up which makes the slopes in figure 3(*a*) decrease slightly below 1.

Figures 4(*a* and *b*) give the results for the temporal variance σ^2. In keeping with the work of Smith (1981), the variance is largest when the discharge is located at the shallow bank. Also, the magnitude of the difference in variance means that the concentration is influenced strongly by the source location. At the shallow bank the approach to the asymptote is relatively slow. Thus figure 4(*a*) extends to twice the downstream distance of all the other figures. This slower response is a consequence of the low value of κ_{22} which delays outwards or inwards diffusion of material.

8. Test of the two-mode approximation

When we integrate-out the z-structure the transverse diffusion equations (4.7*a*, 5.9*a*) for the auxiliary functions G, $G^{(2)}$ take the forms

$$\frac{\mathrm{d}}{\mathrm{d}y}\left(h \parallel \kappa_{22} \parallel \frac{\mathrm{d}G}{\mathrm{d}y}\right) = -h\left(1-\frac{\parallel u \parallel}{\bar{u}}\right), \tag{8.1a}$$

$$\frac{\mathrm{d}}{\mathrm{d}y}\left(h \parallel \kappa_{22} \parallel \frac{\mathrm{d}G^{(2)}}{\mathrm{d}y}\right) = h\frac{\parallel u \parallel}{\bar{u}}\bar{G} - h\left(1-\frac{\parallel u \parallel}{\bar{u}}\right)G, \tag{8.1b}$$

with

$$h \parallel \kappa_{22} \parallel \frac{\mathrm{d}G}{\mathrm{d}y} = h \parallel \kappa_{22} \parallel \frac{\mathrm{d}G^{(2)}}{\mathrm{d}y} = 0 \quad \text{on } y = y_{\mathrm{R}}, y_{\mathrm{L}}, \tag{8.1c}$$

and

$$\int_{y_{\mathrm{L}}}^{y_{\mathrm{R}}} h \parallel u \parallel G \,\mathrm{d}y = \int_{y_{\mathrm{L}}}^{y_{\mathrm{R}}} h \parallel u \parallel G^{(2)} \,\mathrm{d}y = 0. \tag{8.1d}$$

For the triangular topography (7.3) with the model (7.2*a*, *b*) for the velocity and diffusivity distributions, it can be verified that

$$G = t_{\mathrm{c}}\left\{\frac{4}{21} - \frac{2}{5}\left(\frac{y}{B}\right)^{\frac{1}{2}} + \frac{1}{5}\frac{y}{B}\right\}, \tag{8.2a}$$

$$G^{(2)} = t_{\mathrm{c}}^2\left\{\frac{37}{1764} - \frac{8}{105}\left(\frac{y}{B}\right)^{\frac{1}{2}} + \frac{18}{175}\frac{y}{B} - \frac{14}{225}\left(\frac{y}{B}\right)^{\frac{3}{2}} + \frac{1}{70}\left(\frac{y}{B}\right)^{2}\right\}. \tag{8.2b}$$

The seven integrals required in the two-mode analysis of §6 have the values

$$\left.\begin{aligned} \bar{G} &= \frac{2}{525}t_{\mathrm{c}}, \quad \frac{\overline{uG^2}}{\bar{u}} = \frac{1}{4410}t_{\mathrm{c}}^2, \quad \overline{G^{(2)}} = \frac{2}{11025}t_{\mathrm{c}}^2, \\ \frac{\overline{uGG^{(2)}}}{\bar{u}} &= \frac{797}{76403250}t_{\mathrm{c}}^3, \quad \frac{\overline{(\bar{u}-u)GG^{(2)}}}{\bar{u}} = \frac{421}{38201625}t_{\mathrm{c}}^3, \\ \frac{\overline{uG^{(2)2}}}{\bar{u}} &= \frac{445639}{834323490000}t_{\mathrm{c}}^4, \quad \overline{G^{(2)2}} = \frac{133237}{106964550000}t_{\mathrm{c}}^4 \end{aligned}\right\} \tag{8.3}$$

Substituting these results into the quadratic equations (6.7) we obtain the two roots

$$\mu_1 = 16.688\frac{t_{\mathrm{c}}}{\bar{u}}, \quad \mu_2 = 44.20\frac{t_{\mathrm{c}}}{\bar{u}}. \tag{8.4}$$

The exact analysis (7.4*a*, 7.5) yields the exact eigenvalues

$$\mu_1 = 16.609\frac{t_{\mathrm{c}}}{\bar{u}}, \quad \mu_2 = 41.36\frac{t_{\mathrm{c}}}{\bar{u}}. \tag{8.5}$$

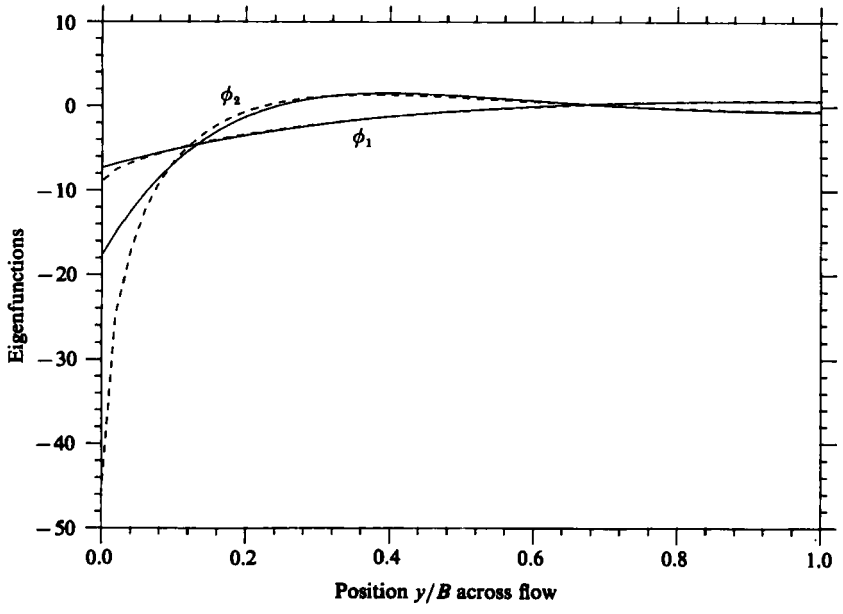

FIGURE 5. Exact (——) and approximate (----) modal shapes for a shallow triangular channel.

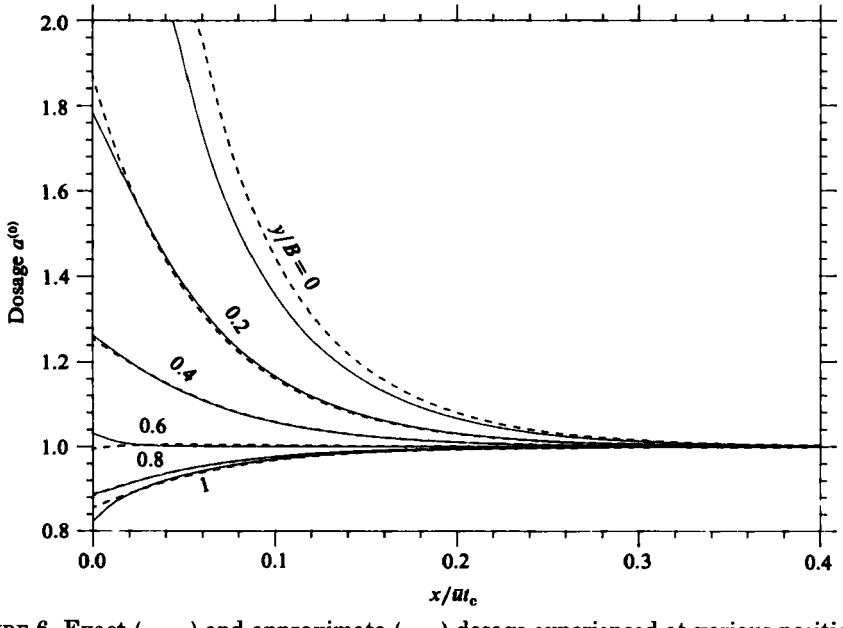

FIGURE 6. Exact (——) and approximate (----) dosage experienced at various positions y across the flow downstream of a uniform discharge.

Thus, there is better than one per cent accuracy for the leading eigenvalue μ_1, but a considerably less accurate estimate for the second eigenvalue μ_2. Figure (5) gives the corresponding comparisons of the exact and approximate modes. As is usual for eigenvalue problems, the eigenfunctions are less accurate than the eigenvalues.

The largest errors in the mode shapes are at the boundaries. Thus, the most

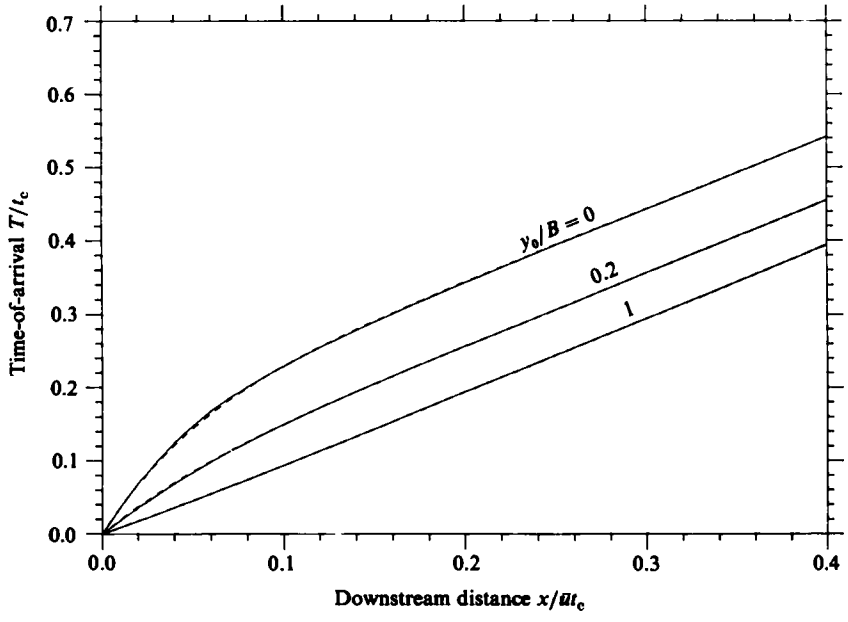

FIGURE 7. Exact (——) and approximate (----) temporal centroid downstream of a uniform discharge.

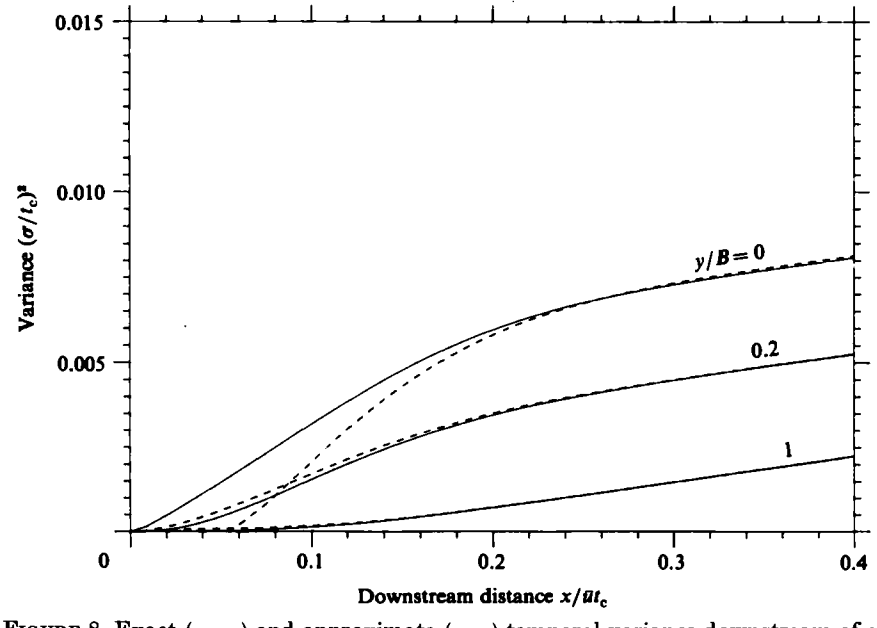

FIGURE 8. Exact (——) and approximate (----) temporal variance downstream of a uniform discharge.

stringent test of the two-mode approximation is to consider the concentration experienced at the boundaries. These are precisely the conditions investigated in figures (2–4). The dashed curves show that close to the discharge the approximations are unreliable. However, most of the approach to the asymptotic form is well-reproduced, and the asymptotes are exact.

The most widely studied discharge condition is one which is uniform across the flow. Figures (6.8) show the dosage, centroid and temporal variance in this case at several locations y/B across the flow. This is the mode of presentation used by Tsai & Holley (1978, figure 2). By contrast with the worst case results (figures 2–4) exhibited above, the accuracy of the two-mode approximation is quite impressive even at small distances from the discharge.

9. Concluding remarks

The work of Tsai & Holley (1978), Chatwin (1980), and that presented here, demonstrate how temporal moments can be used in numerical predictions, in the analysis of field data, and to obtain exact analytic results. On all accounts the temporal approach is of similar complexity, and hence is a genuine alternative to the longer-established spatial approach to contaminant dispersion.

One facet of the exact analysis is that it can provide canonical examples for the testing of numerical methods. More substantially, the exact form of solutions can give valuable insight for the qualitative understanding of the dispersion process, and towards the development of efficient approximation schemes. For example in §6 above it is shown that from the velocity profile $u(y, z)$ and two readily calculable auxiliary functions $G(y, z)$, $G^{(2)}(y, z)$ it is possible to construct a two-mode approximation. By design, the asymptotic form at large x is exact and the approach to the asymptote is reasonably accurate.

The financial support of the Royal Society is gratefully acknowledged.

REFERENCES

ARIS, R. 1956 On the dispersion of a solute in a fluid flowing through a tube. *Proc. R. Soc. Lond.* A **235**, 67–77.

CHATWIN, P. C. 1970 The approach to normality of the concentration distribution of a solute in solvent flowing along a straight pipe. *J. Fluid Mech.* **43**, 321–352.

CHATWIN, P. C. 1971 On the interpretation of some longitudinal dispersion experiments. *J. Fluid Mech.* **48**, 689–702.

CHATWIN, P. C. 1980 Presentation of longitudinal dispersion data. *J. Hydraul. Div. ASCE* **106**, 71–83.

FISCHER, H. B. 1973 Longitudinal dispersion and turbulent mixing in open-channel flow. *Ann. Rev. Fluid Mech.* **5**, 59–78.

SMITH, R. 1981 The importance of discharge siting upon contaminant dispersion in narrow rivers and estuaries. *J. Fluid Mech.* **108**, 43–53.

SMITH, R. 1982*a* Gaussian approximation for contaminant dispersion. *Q. J. Mech. Appl. Maths* **35**, 345–366.

SMITH, R. 1982*b* Where to put a steady discharge in a river. *J. Fluid Mech.* **115**, 1–11.

SMITH, R. 1984 Temporal moments for contaminant releases in rivers. *J. Fluid Mech.* **140**, 153–174.

TAYLOR, G. I. 1953 Dispersion of soluble matter in solvent flowing slowly through a tube. *Proc. R. Soc. Lond.* A **219**, 186–203.

THACKER, W. C. 1976 A soluble model of shear dispersion. *J. Phys. Oceanogr.* **6**, 66–75.

TSAI, Y. H. & HOLLEY, E. R. 1978 Temporal moments for longitudinal dispersion. *J. Hydraul. Div. ASCE* **104**, 1617–1634.

YOTSUKURA, N. & SAYRE, W. W. 1976 Transverse mixing in natural channels. *Water Resources Res.* **12**, 695–704.